JOURNAL OF SPACECRAFT AND ROCKETS
Vol. 34, No. 4, July–August 1997

Preflight Testing and Flight Performance of the OEDIPUS-C Tether Force Sensor

Alexander M. Jablonski* and Frank R. Vigneron†
Canadian Space Agency, Saint-Hubert, Quebec J3Y 8Y9, Canada
Ray D. Rhew‡
NASA Langley Research Center, Hampton, Virginia 23681
John L. Bergmans§
CFD Research Corporation, Huntsville, Alabama 35805
and
William R. Whitehead¶ and George Tyc**
Bristol Aerospace Limited, Winnipeg, Manitoba R3C 2S4, Canada

The authors describe preflight calibration and qualification testing of the tether force sensor developed for the Canadian OEDIPUS-C mission flown on Nov. 6, 1995. OEDIPUS stands for observations of electric field distribution in the ionospheric plasma, a unique strategy. The OEDIPUS-C payload was designed as a large double probe for sensitive measurements of weak electric fields in the plasma of the aurora. It was launched using Black Brant XII sounding rocket to a trajectory with an apogee of 843 km, and the length of deployed conducting tether was 1174 m. There were 13 scientific experiments onboard, including the tether dynamics experiment with the tether force sensor as its prime instrument. This instrument is a strain-gauge-based three-axis force transducer that measures the instantaneous tether tension vector. Qualification and environmental testing of the transducer are summarized. The calibration testing of the tether force sensor is presented together with its theoretical background. During preflight testing, sources of errors and secondary performance characteristics were also identified. The tether force sensor flight performance met designed flight requirements. The representative tether force sensor flight data including time histories of tether force components are presented.

Nomenclature

F_x, F_y, F_z = components of the force applied to the sensor, lb
K = diagonal matrix of sensitivity coefficients
$K_{x,x} = 1/k_{x,x}$ = example of sensitivity coefficient in X-direction gauge due to load applied in the same direction, lb/(V/V)
$\hat{K}$ = matrix of interaction coefficients
$k_{x,i}$ = first-order interaction coefficient in gauge i due to load applied in the X direction, (V/V)/lb
$k_{x^2,i}$ = second-order interaction coefficient in gauge i due to load applied in the X direction, (V/V)/lb
$\boldsymbol{k}_x$ = vector of the first-order interaction coefficients due to load applied in the X direction
$\boldsymbol{k}_{x^2}$ = vector of the second order interaction coefficients due to load applied in the X direction
$\boldsymbol{k}_{xy}$ = vector of cross-coupling interaction coefficients on each gauge output due to load applied in the X direction
M_x, M_y, M_z = components of the moment applied to the sensor, lb · m
$S_{\max}$ = maximum force-vector error for specific type of gauge
$S(\nu)$ = error in measurement of the angle between the tension vector and vertical of the sensor
$\boldsymbol{X}$ = vector of first-order applied loads
$\hat{\boldsymbol{X}}$ = vector of first- and second-order applied loads

Received Aug. 29, 1996; revision received Feb. 21, 1997; accepted for publication Feb. 24, 1997.

*Senior Research Scientist. Member AIAA.
†Consultant. Senior Member AIAA.
‡Research Engineer.
§Research Engineer. Member AIAA.
¶Electrical Engineer. Member AIAA.
**Mechanical Engineer. Member AIAA.

Introduction

THE OEDIPUS-C (observations of electric field distribution in the ionospheric plasma—a unique strategy) mission was successfully launched on Nov. 6, 1995, into a suborbital orbit trajectory using the Black Brant XII sounding rocket from the Poker Flat Research Rocket Range near Fairbanks, Alaska. The altitude at apogee reached 843 km, and a 1174-m tether was successfully deployed. Onboard instruments on both forward and aft subpayloads performed well, including the tether force sensor (TFS) situated at the forward end of the aft subpayload. The scientific instruments included the following instruments on the forward payload: high-frequency exciter, energetic-particle instrument, thermal ion detector, triaxial flux-gate magnetometer, plasma probe; and on the aft payload: receiver for exciter, energetic-particle instrument, thermal ion detector, triaxial flux-gate magnetometer, plasma probe, ram sensor, tether current monitor, and TFS.[1] There were also required subsystems [power, telemetry, instrument control, attitude control system (ACS) booms] as well as the tether deployer and tether cutters, the pneumatic system for payload separation, and other subsystems such as the attitude video camera (AVC) on both payloads. The TFS, flown as a primary flight instrument, was developed as a part of the Tether Dynamics Experiment (TDE), which was sponsored by the Space Technology Branch of the Canadian Space Agency (CSA). The main objectives of the TDE were to develop a comprehensive understanding of the complex dynamics of the spinning tethered configuration with flexible appendages, and to support the payload development. The OEDIPUS-C mission was sponsored by the Space Science Program of the CSA and was developed as a joint program with NASA.

The TFS design was derived from the tethered satellite force transducer developed by NASA Langley Research Center for the Small Expandable Deployer System (SEDS) designed for the Delta II rocket to deploy an end mass.[2] The SEDS sensor was designed to measure tensions up to 4.50 lb in each direction and resolve

tensions as low as 0.0004 lb. The TFS was, in contrast, designed to measure lower tensions, in the 0–1 lb range, and with a resolution of 0.000045 lb. The SEDS-1 and SEDS-2 were orbital missions and were designed for higher tensions than the OEDIPUS class suborbital missions. The TFS measured three-axis tension vector components at the tether attachment point to the aft subpayload. This strain-gauge-based instrument uses two independent sets of gauges: foil gauges and piezoresistive (PR) gauges. The details of the performance requirements, design constraints, flexure and strain-gauge design, and mechanical and electrical component design have been presented already.[3]

This paper focuses on the preflight testing of the TFS and its performance during the flight as assessed during initial postflight analyses. The preflight testing included the precalibration testing, sensor environmental tests, the final calibration performed together with NASA at Modern Machine & Tool Co. (MM&T), and sensor integration tests.

The environmental tests included vibration, pin-puller, postvibration calibration checkout, and vacuum tests.[4]

Vibration tests covered the following standard tests. An initial sine survey (0.25 g) was done to identify resonances in the instrument. It was found that, after the 6.35 g-rms random shake, a small, just-tolerable shift in the zero level of the instrument had occurred. Thus, sinusoidal (0.25 g) and random (up to 6.3 g) acceleration loadings were applied in succession to the TFS in all three axes. Natural frequencies for the random vibration tests were identified using fast Fourier transforms (FFTs) applied to the sampled data.

The pyro pin-puller test was done to assure acceptable performance of this subsystem. Pin pullers were initiated by the pyro subsystem to activate the TFS flexure, which was held by them as during the launch. Some of them experienced outgassing, which was reduced by the use of an appropriate type of coating for them and also for the tether attachment point. Postvibration calibration checkout tests were also carried out. The standard vacuum test completed the environmental tests of the TFS.

The final calibration tests involved applying full-scale loads in small increments and removing them in the same manner (for single-component loadings, two-component loadings, proof loadings, and other loadings to check secondary characteristics of the sensor).[5] The theoretical background of the calibration tests is described in this paper along with examples.

Examples of flight data examples are also presented, and the sensor flight performance is assessed. More description of flight dynamics of the OEDIPUS configurations is presented in the companion papers.[6,7]

The flexure element was fabricated from 7075-T6 aluminum, which is a high-strength aluminum and satisfies the nonferrous-material requirement. The TFS instrument was machined using the wire electrical-discharge machine system from a single piece to attain high-accuracy manufacturing.

TFS Description and Flight Requirements

The TFS location is shown in Fig. 1. Figure 2 shows the flexure gauge, and Fig. 3 shows the designed housing where the flexure is installed. The double-frame geometry utilizes the lower stage (Fig. 2), with four small beams that measure the lateral loads, and the upper stage, with two small beams that measure the axial load. The upper-stage beams (Fig. 2) are 1.5 in. long, 0.4 in. wide, and 0.03 in. thick. The foil gauges are mounted 0.125 in. from the end of the beam, and the PR gauges are mounted 0.53 in. from the end. The beams are also sized to give approximately 500 $\mu\varepsilon$ ($1\ \mu\varepsilon = 10^{-6}$ in./in.). The PR gauges are located toward the middle of the beam, where strain levels are reduced to 200 $\mu\varepsilon$. The compliance in the Z direction was calculated to be 0.16 in. The lower-stage beam design was complicated by the fact that the stage must have compliance in two orthogonal directions. The overall length of the beam is 2.3 in., and the full-scale deflection at the top plate is 0.012 in. The strain levels due to the applied full-scale loads were calculated to be at 220 $\mu\varepsilon$ for the PR gauges and 508 $\mu\varepsilon$ for the foil gauges, whereas the strain level at the hinge area of the secondary beam was calculated at only 462 $\mu\varepsilon$. The calculated compliances along the X and Y axes were 0.016 and 0.021 in., respectively. The flexure had a special integral deflection stop feature, and there were setscrews to immobilize the flexure element (Fig. 2) before it was placed in a special housing.

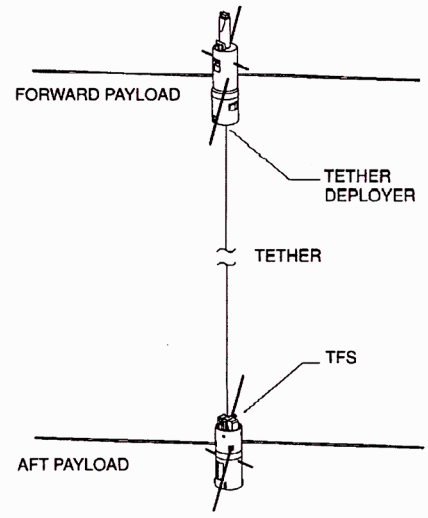

Fig. 1 TFS location in OEDIPUS-C payload.

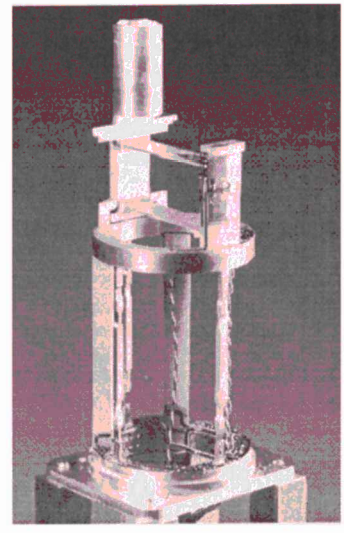

Fig. 2 TFS flexure with foil and PR gauges.

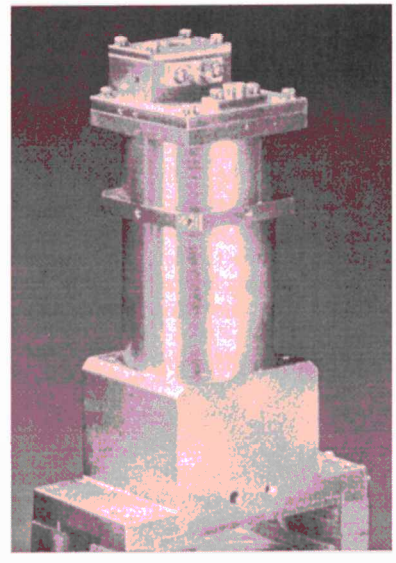

Fig. 3 TFS housing of the flexure.

The major flight requirements for the TFS were to measure the tension throughout the major portion of the flight, including an initial spike due to separation forces, a small variation during deployment, and the fully deployed state up to tether cutting from both ends. A tether cutter on the TFS end was designed to cut the tether without

applying any additional force on the TFS. Based on the nominal tension profile developed in the preflight phase of the project, the TFS measurement requirements were as follows: 1) axial load, full scale, ±1 lb; 2) lateral load, full scale, ±0.5 lb; 3) accuracy, 0.1% of full scale; 4) frequency response, 1 Hz (12 Hz desired); 5) maximum survival tension, 2.2 lb; and 6) sample rate, 100 samples/s.

Several compatibility factors were also included in the TFS, along with survivability due to the launch of the Black Brant XII sounding rocket. They were as follows: the geometrical compatibility (the TFS was to fit between two instruments on the top end of the aft subpayload), magnetic cleanliness, minimum mass, survival through shock and vibration and through temperature change during the launch and the flight, allowance for a point connection to the tether, minimum outgassing for all materials selected, and minimum tether resistance and TFS capacitance (the tether associated electrical signals had to be passed through the TFS to one of the scientific instruments).

Qualification and Environmental Testing

Precalibration testing was carried out before standard environmental tests (vibration and vacuum) and consisted of initial inspection after receiving, precalibration actions, setting overload stops, PR-gauge temperature compensation, printed circuit board amplifier installation, and preliminary functional tests. Special procedures were applied for storage and shipping of the TFS. The TFS sensor went through vibration tests along all three axes, using the BBXII test profiles, with pyro pin pullers installed to ensure survival during the launch. The pin pullers were also fired after vibration tests to confirm that they would fully release the flexure after being stressed during the launch. A basic calibration, checking sensitivity and zero offset, was performed before and after the vibration and pin-puller tests. Finally, a vacuum test was performed to simulate operation in a thermally nonconvective environment so as to investigate the TFS internal heating.

The TFS was an extremely sensitive instrument. Thus, the vibration test was carried out with precautions. First, an initial sine-wave survey ($\frac{1}{4}$ g) was performed to identify resonances. Then, progressively higher random shake levels were run while carefully monitoring outputs and performing health checks after each run. It was found that in the 6.35 g-rms random-shake profile, a small zero shift of the instrument had occurred. Subsequent higher-leve shakes were not performed, to avoid damage to the sensor. Because there was no spare TFS flexure and because the TFS was classified as a secondary (noncrucial) hardware component, it was decided to proceed on the assumption that the TFS would survive the launch. Then, the sinusoidal (0.25 g) and random (up to 6.3 g) acceleration loadings were applied in succession to all three axes. There were altogether 12 runs (11 vibration runs and one pyro firing test). The frequencies of the sinusoidal sweep tests were from 2000 to 15 Hz in 115 s. The acceleration levels of the random frequency tests were achieved in four discrete steps to the 6.3 g peak. Natural frequencies were then identified using FFT.

The lowest frequency was identified for the sinusoidal sweep in channels F_y and P_y: 60 Hz. The highest frequency, 2500 Hz, was present in random sweeps in both X and Y directions at the 6.3 g level. It was assumed that this frequency was due to an internal resonance of the TFS flexure. This peak was prominent in the Y direction, and visible also in the X direction. It did not occur in the Z direction.

The vacuum test showed how the TFS thermal control system is affected by a vacuum condition. The temperature increase was measured to be approximately 0.020°C/min. The thermal controller was found not to be sufficient to fully stabilize the temperature. However, for the short time of the flight the change was assessed to be acceptable.

Other tests carried out included a series of integration tests to allow testing of the A/D converter and pulse-code modulator encoder interface for the proper coordination of the telemetry data to be transmitted during the flight. The final test was an alignment test to ensure correct relative orientation of the TFS geometrical axes to the overall aft-payload axes.

A photograph of the TFS integrated into the payload is shown in Fig. 4.

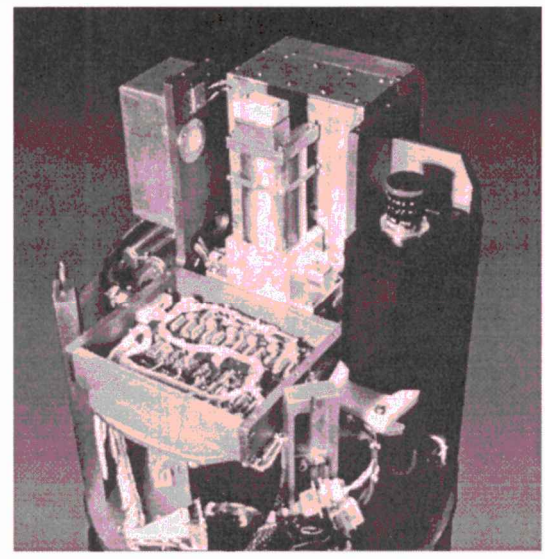

Fig. 4 TFS integrated in the aft payload.

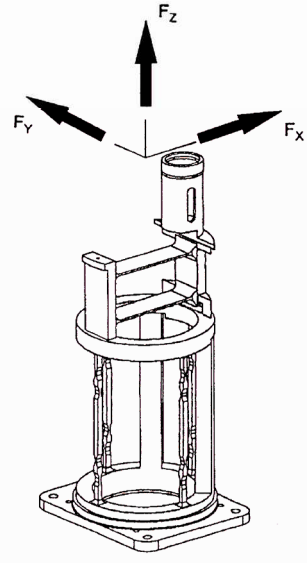

Fig. 5 Tether force components of the TFS.

Calibration Background and Testing

NASA Langley Research Center has extensive knowledge and experience in the calibration of multicomponent balances for testing aircraft models in wind tunnels. This know-how was used to develop the SEDS tether force transducer and subsequently the OEDIPUS-C TFS instrument. The background of the calibration theory is summarized below. The system of the force components of the TFS is presented in Fig. 5.

In general, the output from a strain-based force sensor is a function of all possible combinations of force and moment loads acting. This can be expressed as

$$\boldsymbol{\theta} = f(F_x, F_y, F_z, M_x, M_y, M_z) \tag{1}$$

An interaction equation for the gauge output assuming there is no moment interactions applied is

$$\boldsymbol{\theta} = [\boldsymbol{k}_x, \boldsymbol{k}_{x^2}, \boldsymbol{k}_y, \boldsymbol{k}_{y^2}, \boldsymbol{k}_z, \boldsymbol{k}_{z^2}, \boldsymbol{k}_{xy}, \boldsymbol{k}_{xz}, \boldsymbol{k}_{yz}] \times [X, X^2, Y, Y^2, Z, Z^2, XY, XZ, YZ]^T \tag{2}$$

where $\boldsymbol{\theta}$ is a vector of strain-gauge outputs as defined earlier, $[X, X^2, \ldots, YZ]$ is a vector of applied loads, and $\boldsymbol{k}_x = [k_{x,x}, k_{x,y}, k_{x,z}]^T$ and $\boldsymbol{k}_{x^2} = [k_{x^2,x}, k_{x^2,y}, k_{x^2,z}]^T$ are vectors of first- and second-order interaction coefficients for each gauge output due to a load applied in the X direction. The first and second interaction terms due to Y and Z loads have a similar form. Similarly, the vector $\boldsymbol{k}_{xy} = [k_{xy,x}, k_{xy,y}, k_{xy,z}]^T$ represents cross-coupling interaction on each gauge output due to two simultaneous loads in the X and Y

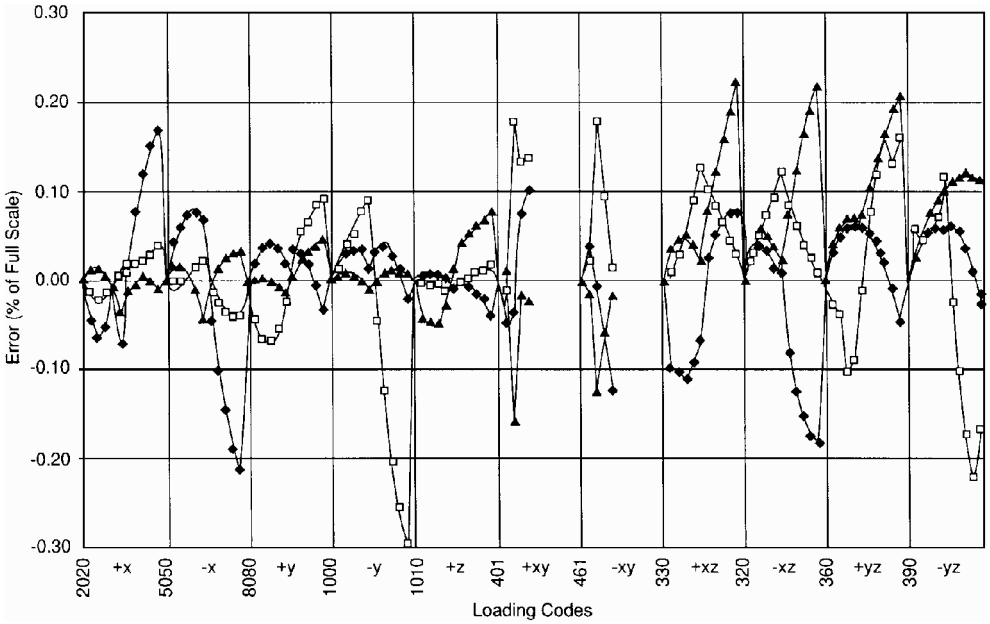

Fig. 6 Error between computed and actual TFS loading for loads applied during calibration. Computed load is based on foil-gauge output: ♦, x; □, y; and ▲, z.

directions. The vectors $\boldsymbol{k}_{xz}$ and $\boldsymbol{k}_{yz}$ have a similar form. Assuming no moment interaction, there are 27 terms that must be computed to calibrate the sensor.

The desired output of the sensor is a measure of the applied load. The sensitivity constants are normalized as follows: $K_{x,x} = 1/k_{x,x}$, $K_{y,y} = 1/k_{y,y}$, and $K_{z,z} = 1/k_{z,z}$. Multiplying rows 1, 2, and 3 of Eq. (2) by $K_{x,x}$, $K_{y,y}$, and $K_{z,z}$, respectively, results in the normalized interaction coefficients, e.g., $K_{y,x} = k_{y,x}/k_{x,x}$. Rearranging results in the following matrix equation:

$$\boldsymbol{X} = K\boldsymbol{\theta} - \hat{K}\hat{\boldsymbol{X}} \tag{3}$$

where $\boldsymbol{X}$ is a vector of first-order applied loads, K is a diagonal matrix of sensitivity coefficients, and $\boldsymbol{\theta}$ is a vector of strain-gauge outputs as defined earlier. $\hat{K}$ is a matrix of interaction coefficients given by

$$\hat{K} = \begin{bmatrix} 0 & K_{x^2,x} & K_{y,x} & K_{y^2,x} & K_{z,x} & K_{z^2,x} & K_{xy,x} & K_{xz,x} & K_{yz,x} \\ K_{x,y} & K_{x^2,y} & 0 & K_{y^2,y} & K_{z,y} & K_{z^2,y} & K_{xy,y} & K_{xz,y} & K_{yz,y} \\ K_{x,z} & K_{x^2,z} & K_{y,z} & K_{y^2,z} & 0 & K_{z^2,z} & K_{xy,z} & K_{xz,z} & K_{yz,z} \end{bmatrix} \tag{4}$$

and $\hat{\boldsymbol{X}} = [X, X^2, Y, Y^2, Z, Z^2, XY, XZ, YZ]^T$ is a vector of first- and second-order loads applied to the TFS.

In iterative form, Eq. (3) can be expressed as follows:

$$\boldsymbol{X}_n = K\boldsymbol{\theta} - \hat{K}\hat{\boldsymbol{X}}_{n-1} \tag{5}$$

where $\boldsymbol{X} = 0$.

The calibration testing focuses on applying known loads to the sensor and recording the gauge output. The gauge outputs and load values are then used to compute numerical values for all elements of the matrices K and $\hat{K}$ using the linear regression technique. The TFS calibration steps include 1) calculation of sensitivity and interaction coefficients for the series of single and multicomponent load cases; 2) calculation of the loads that are applied during calibration; 3) comparison of calculated loads with actual loads; and 4) expression of the differences as percentage errors (accuracies). Also, sensitivities and interaction coefficients were calculated for TFS temperature readings.

The calibration testing was carried out jointly by NASA Langley Research Center, CSA, and Bristol Aerospace Ltd. at the NASA Langley contractor facility in Newport News, Virginia.[5] The calibration process involved applying precision weights to the sensor and recording corresponding voltage output. The relationship between sensor output and loading, Eq. (5), was used for the engineering data reduction. This conversion equation was also applied to assess the errors. The errors for each calibration load, using foil- and PR-gauge outputs, are shown in Figs. 6 and 7, respectively. The temperature correction is included in the results presented here. The single- and two-component loadings were used to determine the sensitivities and interaction coefficients; the proof loadings were used as independent verifications of the calculated coefficients. Figure 6 presents the percentage error with respect to full scale for foil gauges between computed and actual TFS loading readings for loads applied during calibration. Altogether 11 cases for loading are presented: in the $+X$ direction (code 2020), in the $-X$ direction (code 5050), in the $+Y$ direction (code 8080), in the $-Y$ direction (code 1000), in the $+Z$ direction (code 1010), in the two directions $+XY$ (code 401), etc. Figure 7 presents the same comparison for the PR gauges. Plots are given for foil and PR gauges in the X, Y, and Z directions. For multiaxial loading, the errors are higher than for uniaxial loading.

Proof loadings involved testing using specially designed angle blocks. These loadings were performed by rotating the TFS and applying a single load with an angle block inducing multiaxis loads on the instrument. A full list of sensitivity and interaction coefficients with the temperature controller on (the temperature was set to 30°C) is presented in Table A1 in the Appendix. An example of the calculation of the load based on foil-gauge outputs using sensitivities and interactions listed in Table A1 is provided in Ref. 5. T_L and T_U are two measurements of the temperature inside the TFS case (T_L in the lower portion and T_U in the upper portion).

A load-magnitude accuracy analysis was performed.[5] In the case of foil gauges, an estimated accuracy was ±0.20−0.22% of full scale, and for PR gauges it was 0.60–0.63% of full scale. The full-scale voltage for the X and Y axes is 4 V; the nominal full scale for the Z axis is 2 V.

The estimated maximum force-vector errors from proof-load testing for foil and PR gauges are

$$S_{\max}(\text{foil}) = \pm 0.002\,\text{lb} \qquad S_{\max}(\text{PR}) = \pm 0.007\,\text{lb}$$

An estimate of the error in the measurement of the angle between the tension vector and vertical is

$$|S(\nu)| = \frac{|S_{\max}|}{F}\frac{180}{\pi}\,\text{deg} \tag{6}$$

It shows that the angular error will increase rapidly for small force readings below 0.1 lb (see Fig. 8).

The following secondary performance characteristics were also assessed within the scope of calibration testing: moment sensitivity,

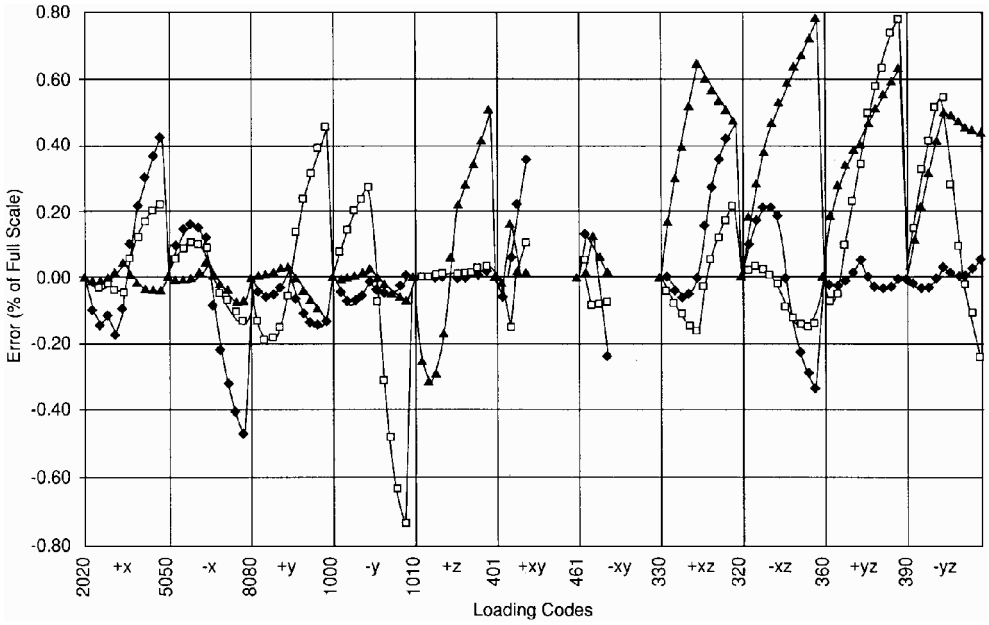

Fig. 7 Error between computed and actual TFS loading for loads applied during calibration. Computed load is based on PR-gauge output: ♦, *x*; □, *y*; and ▲, *z*.

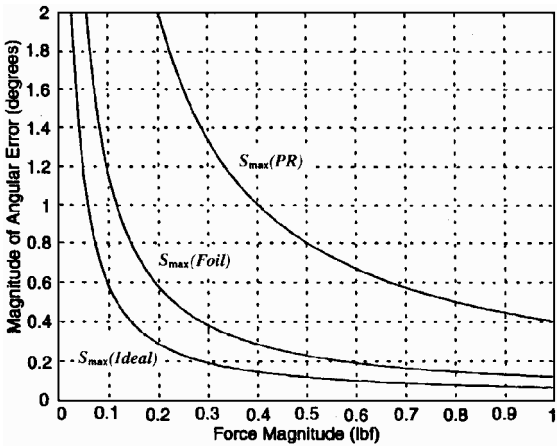

Fig. 8 Magnitude of estimated angular error for foil and PR gauges and desired TFS angular error.

hysteresis and zero shift, response to a step load, long-term performance, multiday zero reading, temperature sensitivity, and also reference-block alignment. Herein, the following tests are briefly discussed: step-response, hysteresis/zero-shift, moment-sensitivity, and long-term test.[5]

The step-responsetest was performed to examine and characterize the change in the gauge output as a function of time when a constant load is applied. This behavior, sometimes referred to as gauge creep, is here called gauge relaxation. The test involved applying the full load of 0.5 lb (or 1.0 lb) in the positive direction along an axis, recording an output for a period of time, removing the load, and again recording an output. The corresponding changes in foil- and PR-gauge outputs are presented in Fig. 9 for the step loading from 0.0 to 0.5 lb in the $+X$ direction and in Fig. 10 for unloading. Figure 9 illustrates the foil-gauge outputs from three tests when the sensor was subjected to a 0.5-lb load, and Fig. 10 illustrates the same tests during unloading in the same direction. The test involved applying the full-scale load in the positive direction of the X axis, recording the output for a period of time, removing the load, and again recording the output. The changes in gauge output allow us also to estimate the change in computed load based on these outputs. From the quantitative point of view, the foil gauges and PR gauges have opposite asymptotical outputs. The magnitude of the PR-gauge output change is greater than that of the foil-gauge change, and the signs of the changes are opposite. The largest change was recorded in the Z direction for step load of 0–1 lb. The change for the foil-gauge

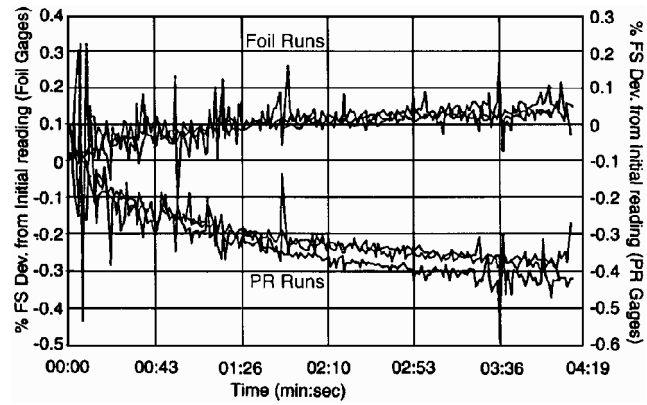

Fig. 9 Change in foil and PR *X*-gauge outputs due to step loading (0.0–0.5 lb) in +*X* direction.

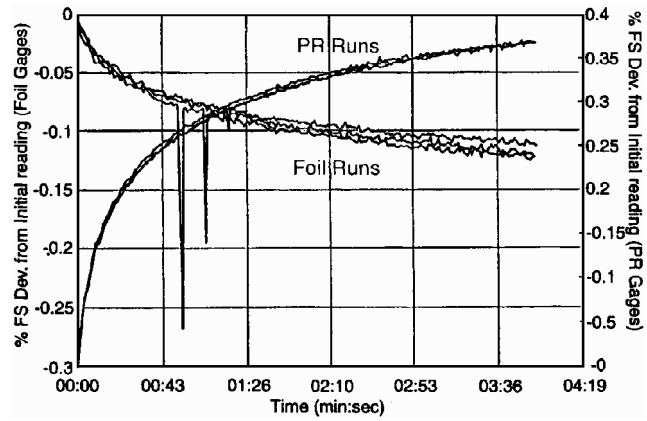

Fig. 10 Change in foil and PR *X*-gauge outputs due to step loading (0.5–0.0 lb) in +*X* direction.

output was +0.0021 lb for loading and −0.0020 lb for unloading. The corresponding changes for PR-gauge output were −0.012 and +0.015 lb. This effect should be considered during the detailed analysis of the OEDIPUS-C flight data. A proposal for reducing the gauge relaxation errors is included in the calibration report.[5]

Cycling loading was applied to each axis to examine hysteresis and zero-shift effects. The test consisted of two cycles of applying and removing (by hand) the full-scale load in steps to a single

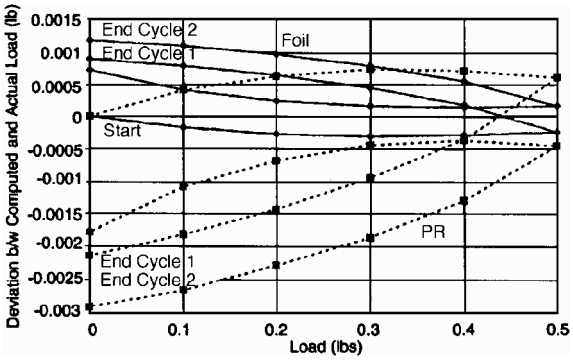

Fig. 11 Errors in computed foil and PR-based X outputs for two cycling loadings along the $+X$ axis.

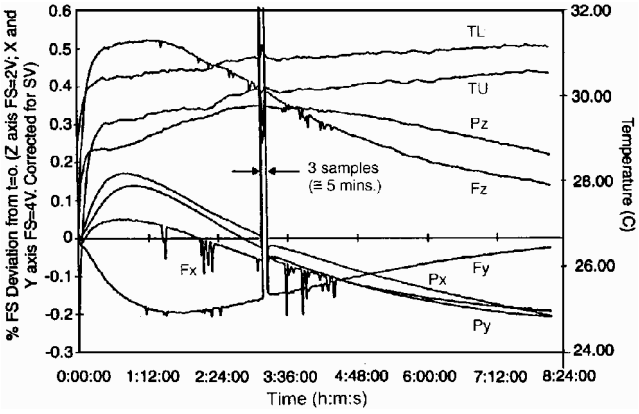

Fig. 12 Long-term test results (from sensor turn-on: $+Z$ axis mounted down; sample period 1.25 min; test performed at MM&T, Aug. 3, 1995).

branch (positive or negative) of each axis. The measured loads were computed from the gauge outputs, and the overall effects were represented by plotting the errors between measured and actual loads. An example of test data is presented in Fig. 11. The tare weight was subtracted from all outputs, resulting in zero initial error.

When the load was removed in similar steps, the errors changed sign. At the end of the first cycle of loading steps, the foil and PR no-load readings had shifted by $+0.00089$ and -0.00215 lb, respectively. At the end of second cycle, these readings had shifted by $+0.00117$ and -0.00291 lb, respectively. Thus, the effects of cycling loading grow with the number of cycles. The implications for the OEDIPUS-C flight data are relatively small, especially in the X and Y (lateral) directions. The zero shift could be more pronounced, depending on the amplitude of the loading cycles, in the Z direction.

The moment sensitivity test was performed at Bristol Aerospace Ltd., and its result was that sensitivity was very small: 0.00011–0.01334 lb/lb · in. for the foil-gauge output and 0.000411–0.030286 lb/lb · in. for the PR-gauge output. The effect of twisting was also assessed, and it appeared to be insignificant, though dependent on the difference between the spin rates of two subpayloads of the OEDIPUS-C configuration.

A long-term test was also performed to investigate the stability of the sensor outputs for both types of gauges over an extended period of time (>8 h). The results of a typical-long term test are presented in Fig. 12. Anomalous points (large spikes) were assumed to be dropouts in readings. This type of dropouts were also present in flight-data outputs.

The predicted levels for both tensions and the flight TFS outputs were also assessed during preflight activities.[3]

TFS Flight Performance and Examples of Flight Data

The TFS data were downlinked in link 3 together with all aft payload engineering data and placed on a CD-ROM by the NASA Goddard Space Flight Center Wallops Flight Facility. This includes all raw data from the TFS instrument: input voltage to temperature controller, lower and upper temperature readings, input voltage to foil and PR gauges, and six outputs of the foil and PR gauges (three foil and three PR in three directions, X, Y, and Z).

The initial processing of the data involved dumping the data from the CD-ROM to the Unix environment, extracting individual TFS components from the data file, and reducing them to engineering units [from counts to voltages and finally to force units (pounds)]. A special program was developed to carry out data reduction.[8] Separate files were created for each gauge: F_x, F_y, F_z, P_x, P_y, and P_z. The plots of time histories of the foil gauges outputs are presented in Figs. 13a–13c. The presented data were based on the raw and unfiltered data from the TFS instrument, and interaction and sensitivity coefficients were obtained from the calibration process. The

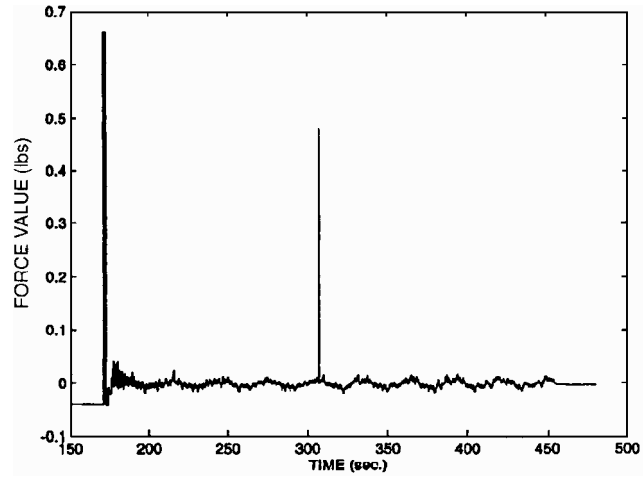

Fig. 13a Foil-gauge X output during OEDIPUS-C flight: F_x vs time.

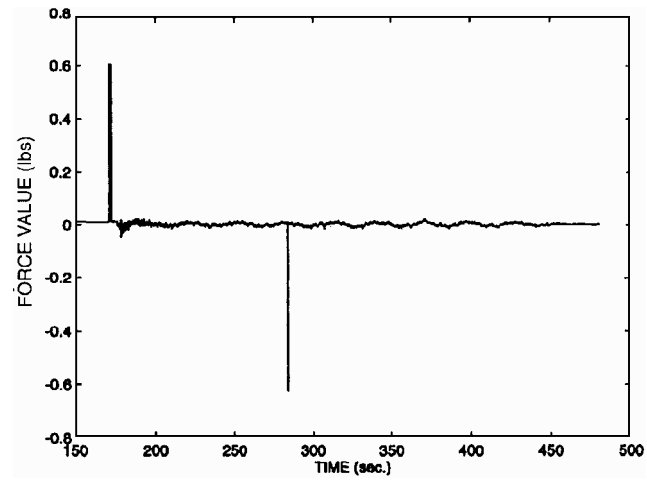

Fig. 13b Foil-gauge Y output during OEDIPUS-C flight: F_y vs time.

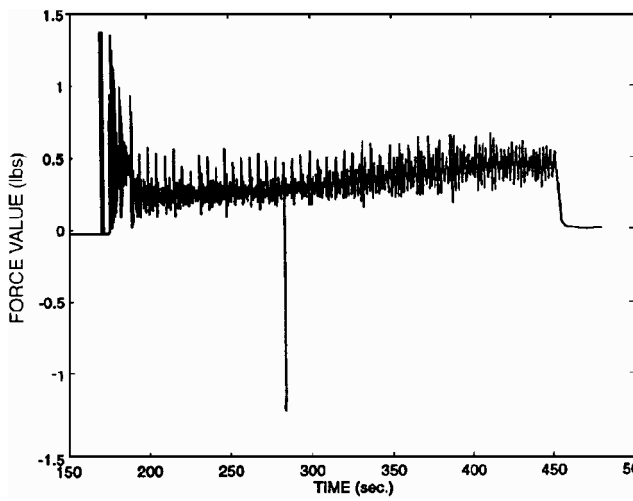

Fig. 13c Foil-gauge Z output during OEDIPUS-C flight: F_z vs time.

initial spike seen in all three plots is due to an in-flight zero calibration. Then, the maximum TFS component in each direction is due to the inertia forces acting on the tether reel. The slow growth of the tension over the next 25–30 s corresponds to the thruster firing during separation. Then, the tension ramps up slowly during the deployment as the braking torque remains constant but the distance from the center of the reel decreases as the tether is deployed. There are also three other spikes on each plot. They may be dropouts in outputs. The data are presented in pounds, and the following formulas are used for conversion from counts to pounds. Assuming that a force of magnitude F in pounds is applied to a particular axis direction of the sensor, the following equation can be used to estimate the gauge output due to an applied load (interaction effects are neglected):

$$F[\text{lb}] = \frac{\text{output}[\text{V}]}{10\,\text{V}} \cdot K \left[\frac{\text{lb}}{\text{V/V}}\right] \tag{7}$$

In the computer program, effects of interaction were also taken into account. The TFS voltage output as a function of applied load can be found from Eq. (1):

$$\text{output} = 10F/K \tag{8}$$

The flight A/D converter displayed the TFS output in counts. The A/D converter is scaled to produce an output of 65,536 counts over an input range of ±2.5 V. The following equation could be used to relate A/D output counts to TFS voltage outputs:

$$\text{output[counts]} = (2F/K) \times 65{,}536 + 32{,}768 \tag{9}$$

The total tether force was calculated from the magnitudes of the three components. Plots of averages of each of the 10 output values are presented for foil gauges and PR gauges in Figs. 14a and 14b, respectively. Expanded plots during the deployment of the tether for foil and PR gauges are presented in Figs. 15a and 15b.

The spike after the sudden drop of the tether tension when the full deployment was reached is present on both plots. It is a result of the recoiling of both subpayloads, as measured at the aft payload, where the TFS instrument was located. Some noise is also presented, especially in the Z direction (Fig. 15). Finally, the plot of the deployment profile is presented as a function of time, based on the data processed from an encoder on the tether reel (Fig. 16).

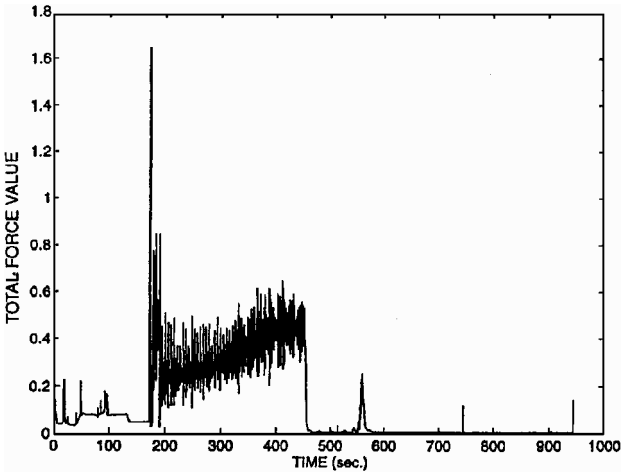

a) Foil-gauge outputs

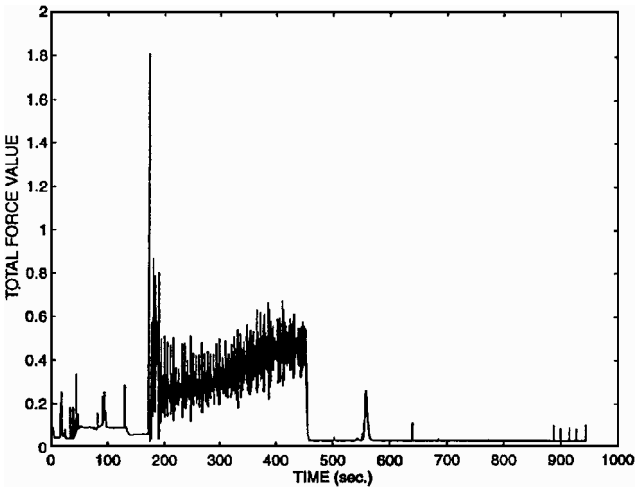

b) PR-gauge outputs

Fig. 14 Total tether force as estimated during OEDIPUS-C flight (zero corresponds to the launch).

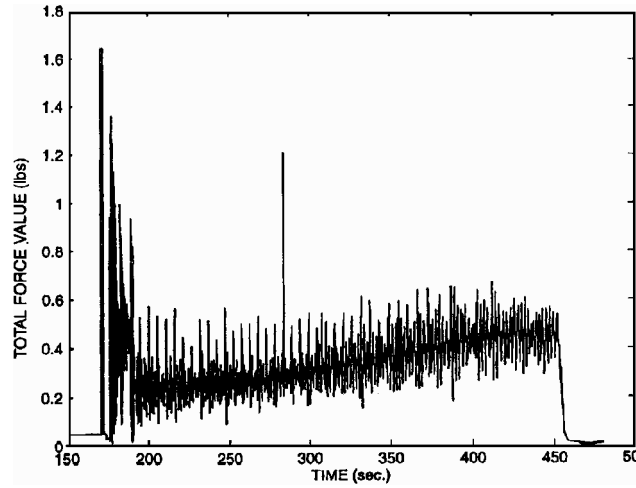

a) Foil-gauge outputs

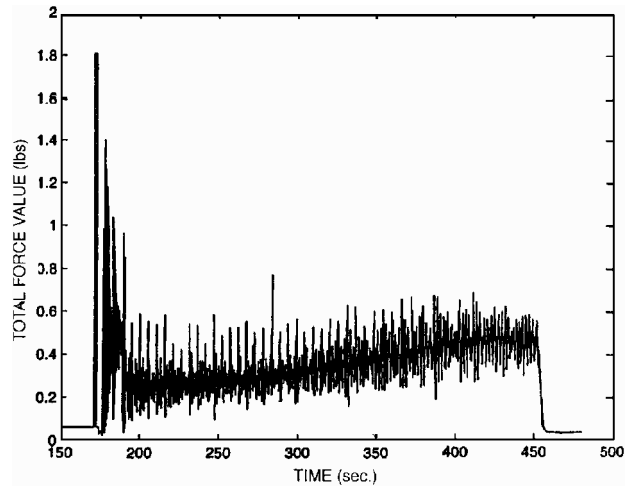

b) PR-gauge outputs

Fig. 15 Total tether force as estimated during deployment of the tether.

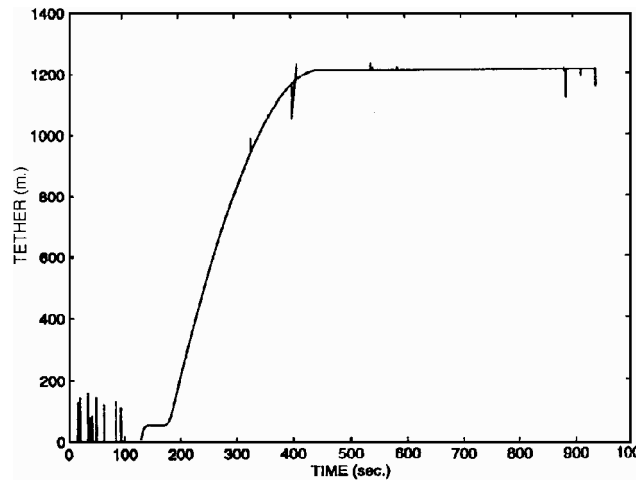

Fig. 16 OEDIPUS-C tether deployment profile.

Table A1 TFS sensitivities and interactions[a]

Controller on (flight temperature)

Quantity	Sensitivities, lb/(V/V)	Av. of T_L, T_U, °C
$K_{x,x}$	2.54623	30.93
$K_{y,y}$	2.51316	30.43
$K_{z,z}$	2.92033	30.54

Interaction terms

i	$K_{i,x}$	% effect	$K_{i,y}$	% effect	$K_{i,z}$	% effect
x	1.00000	100.00	2.25911E−02	2.26	3.07753E−02	1.54
y	−2.00825E−02	−2.01	1.00000	100.00	−8.97055E−03	−0.45
z	3.15503E−05	0.01	5.14165E−04	0.10	1.00000	100.00
x^2	−1.99093E−03	−0.10	−9.36621E−04	−0.05	3.95953E−03	0.10
xy	−1.66598E−03	−0.08	2.05930E−02	1.03	−2.41116E−03	−0.06
xz	−1.24737E−02	−1.25	4.05876E−04	0.04	−4.37477E−03	−0.22
y^2	−1.39940E−02	−0.70	−1.68994E−03	−0.08	−2.04174E−03	−0.05
yz	2.78774E−04	0.03	−1.76286E−02	−1.76	1.44592E−03	0.07
z^2	3.56553E−04	0.07	5.09317E−06	0.00	−2.77103E−03	−0.28

Code	Unloaded zero calculation, V/V			Av. of T_L, T_U, °C
	X	Y	Z	
2020	0.03231	0.00612	0.01575	30.76
5050	−0.03069	0.00485	0.01536	30.88
8080	0.00097	0.03739	0.01576	30.27
1000	0.00194	−0.02648	0.01593	30.40
1010	0.00103	0.00521	0.02151	30.53
1115	0.00081	0.00524	0.01020	31.02
Average	0.00106	0.00539	0.01575	30.64

Controller off (room temperature)

	Sensitivities, lb/(V/V)	Av. of T_L, T_U, °C
$K_{x,x}$	2.54727	26.53
$K_{y,y}$	2.51488	25.69
$K_{z,z}$	5.92088	25.92

Interaction terms

i	$K_{i,x}$	% effect	$K_{i,y}$	% effect	$K_{i,z}$	% effect
x	1.00000E+00	100.00	2.29339E−02	2.29	2.98650E−02	1.49
y	−2.03570E−02	−2.04	1.00000E+00	100.00	−9.41776E−03	−0.47
z	2.94502E−04	0.06	2.75069E−04	0.06	1.00000E+00	100.00
x^2	−2.07937E−03	−0.10	−1.66246E−04	−0.01	8.59112E−04	0.02
xy	——	——	——	——	——	——
xz	——	——	——	——	——	——
y^2	−1.31396E−02	−0.66	4.13436E−06	0.00	−3.23480E−03	−0.08
yz	——	——	——	——	——	——
z^2	2.08566E−04	0.04	−1.40261E−04	−0.03	−2.48074E−03	−0.25

Code	Unloaded zero calculation, V/V			Av. of T_L, T_U, °C
	X	Y	Z	
20	0.03255	0.00620	0.01566	26.37
50	−0.03026	0.00480	0.01543	26.60
80	0.00059	0.03719	0.01553	25.89
100	0.00160	−0.02645	0.01563	25.32
10	0.00095	0.00552	0.02117	26.09
15	0.00092	0.00557	0.00984	25.53
Average	0.00106	0.00547	0.01554	25.97

[a]Foil coefficients (NASA data).

Conclusions and Remarks

Based on the initial assessment of the TFS flight data, the overall TFS instrument performance met the following designed flight requirements both during preflight tests and during flight: accuracy for axial and lateral full-scale loads, ±1 and ±0.5 lb, respectively; frequency response, 1 Hz; sample rate, 100 samples/s. The accuracy of the measurements was lower than expected during preflight assessment but appeared to be sufficient for the flight data. The maximum force recorded by both systems of gauges (1.6–1.8 lb) was lower than the maximum operational value of the instrument (2.2 lb). The instrument was less accurate for the tensions below 0.15 lb, as shown in the recorded data from foil and PR gauges.

The flight data on the TFS demonstrate its correct functioning during flight, and all phases of the flight are recorded: an initial spike due to separation forces, tether deployment, and a sudden drop of the tether tension at the end of the deployment, and also a small restoring force during recoil of the payloads (also recorded by the AVC situated on the aft payload). Some single dropouts are present in all of the recorded data.

The TFS data will provide good insight into tether dynamics, yielding signatures for the dynamics of the subpayloads as well as their associated booms. In future work, these will be extracted from the TFS data using standard FFT techniques.

Appendix: Numerical Results

Numerical values of the TFS sensitivities and interaction are given in Table A1.

Acknowledgments

The authors thank the Space Technology Branch of the Canadian Space Agency for providing the funding and technical support for the development of the OEDIPUS-C TFS. The support of the

engineers and technicians from NASA Langley Research Center, Modern Machine & Tool Co., and Bristol Aerospace Ltd. is gratefully acknowledged. The authors thank also George M. Wood, Science & Technology Co., Hampton, Virginia, formerly with NASA Langley Research Center, for his support and arrangement for providing crucial calibration of the TFS by NASA Langley Research Center staff. Thanks are also due to Michael Valentik, student, University of Waterloo, who performed the initial TFS flight data reduction.

References

[1]James, H. G., and Balmain, K. G., "Space Plasma Experiments with the Tethered OEDIPUS-C Payload," *Proceedings of the 4th International Conference on Tethers in Space* (Smithsonian Inst., Washington, DC), Science and Technology Corp., Hampton, VA, 1995, pp. 1765–1780.

[2]Rhew, R. D., "Development of a Tethered Satellite Force Transducer," *Proceedings of the 39th International Instrumentation Symposium,* Albuquerque, NM, 1993, pp. 287–291 (ISA Paper 93-4764).

[3]Tyc, G., Whitehead, W. R., Phillips, J. L., Pierson, J. G., Jablonski, A. M., and Vigneron, F. R., "Design, Qualification and Calibration of the Tether Force Sensor (TFS) for the OEDIPUS-C Mission," *Proceedings of the Fourth International Conference on Tethers in Space* (Smithsonian Inst., Washington, DC), Vol. 3, Science and Technology Corp., Hampton, VA, 1995, pp. 1793–1807.

[4]Malo, M., "Tether Force Sensor Environmental Test and Payload Integration Test," Bristol Aerospace Ltd., Bristol TR ER 95892/A, Winnipeg, MB, Canada, Dec. 1994.

[5]Bergmans, J. L., and Rhew, R. D., "Tether Force Sensor Calibration Report," Canadian Space Agency, TR OED-TR-95-03, Saint-Hubert, PQ, Canada, Nov. 1995.

[6]Tyc, G., Vigneron, F. R., Jablonski, A. M., Han, R. P. S., Modi, V. J., and Misra, A. K., "Flight Dynamics Results from the OEDIPUS-C Tether Mission," *Proceedings of the AIAA/AAS Astrodynamics Conference* (San Diego, CA), AIAA, Washington, DC, 1996, pp. 39–50 (AIAA Paper 96-3573).

[7]Vigneron, F. R., Chandrashaker, R., Jablonski, A. M., and Tyc, G., "Damped Gyroscopic Modes of Spinning Tethered Space Vehicles with Flexible Booms," *Proceedings of the AIAA/AAS Astrodynamics Conference* (San Diego, CA), AIAA, Washington, DC, 1996, pp. 51–60 (AIAA Paper 96-3574).

[8]Bergmans, J. L., "TFS Flight Data Reduction Program," Canadian Space Agency, Memorandum, Saint-Hubert, PQ, Canada, Jan. 1996.

J. C. Adams Jr.
Associate Editor